IEEE Robotics and Automation Letters (RA-L) paper, presented at ICRA 2024, Yokohama, Japan. Cite as RA-L paper.

Sensorless Transparency Optimized Haptic Teleoperation on the da Vinci Research Kit

Nural Yilmaz[1,3], Brendan Burkhart[1], Anton Deguet[1], Peter Kazanzides[1], Ugur Tumerdem[2,3]

***Abstract*—The da Vinci surgical robot introduced remote control of instruments, providing surgeons with increased dexterity and precision. A major drawback, however, is the loss of sense of touch due to a lack of kinesthetic coupling between the surgical field and the surgeon. This paper presents a framework for sensorless transparency optimized four channel teleoperation. It is sensorless because forces are estimated from existing actuator feedback, with a deep network for dynamics identification. Performance is further optimized by introducing robust acceleration control, with disturbance observers. Experiments performed on the da Vinci Research Kit (dVRK), an open research platform based on the clinically deployed robotic hardware, show improvements in control, force estimation and reflection. The significance is that we demonstrate that high-performance bilateral teleoperation is feasible in clinical systems, without hardware changes, and is available to the dVRK community through a software update.**

***Index Terms*—Surgical Robotics: Laparoscopy, Telerobotics and Teleoperation, Force and Tactile Sensing.**

I. Introduction

ROBOTICALLY assisted minimally invasive surgery (RAMIS) utilizes robotic telemanipulation technology to assist surgeons in minimally invasive procedures. The da Vinci Surgical System (Intuitive Surgical, Sunnyvale, CA) was the first system to receive FDA approval in 2001 and today over 6000 systems are operational globally [1]. Robotic surgery provides improved precision, dexterity and greater range of motion compared to conventional laparoscopy. This is made possible by endoscopic robotic instruments that can be remotely controlled by robotic manipulanda.

However, the benefits are counter-weighted by the loss of haptic feedback from the surgical field, which is one of the most cited limitations of RAMIS systems [2], [3]. Experienced robotic surgeons have learned to estimate forces through visual cues, but it is widely believed that surgical performance would be improved by the addition of haptic feedback. Certain interaction forces in minimally invasive surgery are difficult to gauge with visual cues only, such as contact forces with the beating heart [4], or hidden tumors [5]. Due to a lack of haptic feedback, applying excessive tension/force can result in breakage of suture [6], bending of needles [7] or damage to the tissue.

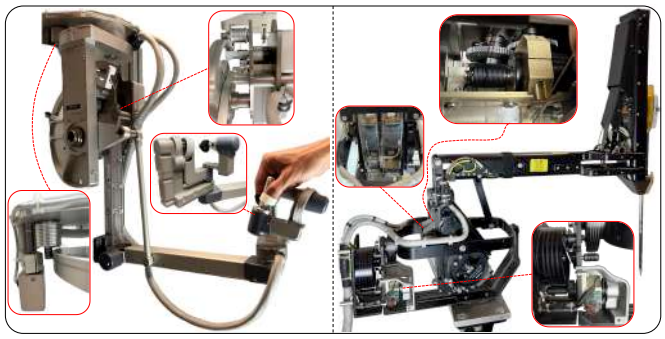

Fig. 1. dVRK Teleoperation System: Master Tool Manipulator (Left), Patient Side Manipulator (Right). Actuators, encoders and capstan transmissions are more clearly visible in red boxes.

There are several technical limitations that prevent interaction forces from being presented to the surgeons with high fidelity and in all degrees of freedom. Most importantly, it is difficult to miniaturize and integrate force sensors in existing instruments. It is also a challenge to estimate forces from robot measurements, due to the nonlinear dynamics of the robots, which are cable driven, highly flexible, work against gravity and interact with the patient body at several locations. The nonlinearity also makes it harder to design stable and transparent bilateral teleoperation controllers.

We have developed a framework to overcome several of the mentioned limitations, and this paper reports the first successful implementation of a force sensorless transparency optimized haptic teleoperation between the Master Tool Manipulator (MTM) and the Patient Side Manipulator (PSM) of the da Vinci Research Kit (dVRK) [8], an open source research version of the da Vinci surgical system (Fig. 1).

II. Related Work

A. Force Sensing and Estimation in Robotic Surgery

A significant hurdle to realizing haptic feedback in robotic surgery is the difficulty in obtaining force measurements from the PSM. Commercially available force sensors are typically too bulky for laparoscopic applications. Miniaturized force sensors with 3/6 degrees-of-freedom (DOF) have been developed [9]–[11], and strain gauges [7], [12], capacitive [13] and optical [14] sensors have also been used, but due to increased

Manuscript received: May 29, 2023; Revised: October 06, 2023; Accepted: October 29, 2023.

This paper was recommended for publication by Editor Pietro Valdastri upon evaluation of the Associate Editor and Reviewers' comments.

[1]Dept. of Computer Science, [2]Dept. of Mechanical Engineering, Johns Hopkins University, Baltimore, MD 21218, USA, [3]Dept. of Mechanical Engineering, Marmara University, Istanbul, 34854, Turkey (email: {nyilmaz2, bburkha4, anton.deguet, pkaz, ugur}@jhu.edu)

Nural Yilmaz was supported by the TUBITAK 2214A International Research Fellowship Program. Ugur Tumerdem was supported by the Fulbright Visiting Scholar Program.

Digital Object Identifier (DOI): see top of this page

IEEE Robotics and Automation Letters (RA-L) paper, presented at ICRA 2024, Yokohama, Japan. Cite as RA-L paper.

IEEE Robotics and Automation Letters (RA-L) paper, presented at ICRA 2024, Yokohama, Japan. Cite as RA-L paper.

integration complexity and sterilization requirements, have not yet found widespread application.

It is also possible to estimate forces without force sensors. The most common method in surgical robotics is based on measurement of the driving current of the actuators. As most robots utilize DC motors, the driving current and load torque can be related by the torque constant [15]. This approach was first used on the Black Falcon [16], then on the da Vinci and dVRK systems in [17]–[23] and Raven open source surgical platform in [24], [25]. In this approach, estimation accuracy depends on the accuracy of current measurement and the torque constant. Alternatively, external force observers with encoder measurements can be used [18], [26]. A common issue in estimation is that external forces may not be fully transmitted to the actuators due to the robot transmission and elasticity. Disturbances such as friction and gravity also have to be filtered out for external force estimation. Friction identification [17], cable tension estimation [24], and model based dynamic identification [18], [20] have all been used to improve force estimation.

In [21], [22], end-to-end machine learning was proposed to estimate external forces on da Vinci systems. In [27], vision data was also added in training to improve force estimation. Since these networks are trained with force sensors under specific conditions, it is not known how well they would generalize to changing operating conditions.

In our previous work, [26], [28], external force estimation using neural networks instead of explicit models was employed to identify robot dynamics. It was also shown in [29] that the neural network training could be augmented by transfer learning to adapt to different robot dynamics, patient/robot interactions at the trocar, and instrument changes. In [30], we demonstrated 7 DOF force estimation (including grip force) on the patient side manipulators.

B. Haptic Teleoperation in Robotic Surgery

While much work has been done on force estimation in robotic surgery, few works demonstrate bilateral/haptic teleoperatiocn on surgical robots. The earliest form of haptic teleoperation on a surgical system made use of the two channel P-P architecture (position exchange and control between the robots) on the Black Falcon [16]. Methods to improve transparency using position exchange on dVRK robots were proposed in [31] and [32].

For direct force feedback teleoperation, force sensing/estimation has been used in some surgical prototypes [4], [26], [33]. On da Vinci systems, strain gauge based sensing [7], and current based force estimation [17], [34] on PSMs have been used. In [**?**], vision augmented force estimation from the PSM was utilized for haptic feedback. All mentioned systems make use of the two channel F-P teleoperation architecture where the MTM is controlled with force feedback from the patient side and the PSM follows the MTM position.

However, neither of these architectures (P-P or F-P) can achieve transparency in bilateral teleoperation [35]. Four channel teleoperation, which requires the exchange and control of both position and force measurements between the robots, was proposed to achieve ideal transparency. The implementation of this architecture would require force sensing and position tracking on both the MTM and PSM [36], which is challenging on the dVRK. Estimating forces and dynamic motion control on the MTM is also difficult due to low structural rigidity, encoder resolutions and actuator torques. In [37], a special 6 DOF force sensor was developed for the MTM, but a bilateral teleoperator was not constructed.

C. Contributions

In this paper, we propose a framework to realize sensorless transparency optimized (four channel) teleoperation on the da Vinci Research Kit. This method could easily be implemented, via a software update, on a large number of robots that are actively being used in surgery or research.

While the four channel architecture has been shown to have excellent performance on teleoperation systems with linear dynamics or negligible non-linearities, few applications on multi-DOF robots exist with no implementation on surgical robots. The proposed method in this paper builds on our recent results on sensorless force estimation as well as bilateral teleoperation [26], [28]–[30] and combines for the first time disturbance observers, neural network based dynamic identification and force estimation, as well as four channel teleoperation. In this paper, for the first time on a da Vinci system:

- Real-time learning based sensorless force estimation on both the PSM and MTM is presented.
- A four channel teleoperation architecture, which is the gold standard in bilateral teleoperation for transparency, is implemented and validated on 6 active DOFs.
- Disturbance observers are implemented for improved position tracking as well as an alternative to force estimation based on motor currents.
- The sensorless four channel teleoperation is compared with other teleoperator architectures and shown to provide significant performance improvements.

III. Method

A. Robot Dynamics and Feedback Linearization

The Euler-Lagrange model of a general robot manipulator can be written as:

$$\mathbf{M}(\mathbf{q})\ddot{\mathbf{q}} + \mathbf{C}(\mathbf{q}, \dot{\mathbf{q}}) + \mathbf{G}(\mathbf{q}) + \mathbf{F}(\dot{\mathbf{q}}) = \boldsymbol{\tau} \tag{1}$$

where $\mathbf{q}, \dot{\mathbf{q}}$ are the joint position/velocity vectors, $\boldsymbol{\tau}$ is the joint torque vector, $\mathbf{M}(\mathbf{q})$ is the inertia matrix, $\mathbf{C}(\mathbf{q}, \dot{\mathbf{q}})$ is the Coriolis and centrifugal torque vector, $\mathbf{G}(\mathbf{q})$ is the gravity vector, and $\mathbf{F}(\dot{\mathbf{q}})$ is the friction vector. Due to the nonlinearity of the dynamics, linear controllers cannot always guarantee good performance or stability. One approach to designing linear controllers for robots is to use feedback linearization with the resolved acceleration control law [38]:

$$\boldsymbol{\tau} = \mathbf{M}(\mathbf{q})\ddot{\mathbf{q}}_{\mathbf{ref}} + \mathbf{C}(\mathbf{q}, \dot{\mathbf{q}}) + \mathbf{G}(\mathbf{q}) + \mathbf{F}(\dot{\mathbf{q}}) \tag{2}$$

$$\ddot{\mathbf{q}}_{\mathbf{ref}} = \ddot{\mathbf{q}}_{\mathbf{d}} + \mathbf{K}_{\mathbf{d}}(\dot{\mathbf{q}}_{\mathbf{d}} - \dot{\mathbf{q}}) + \mathbf{K}_{\mathbf{p}}(\mathbf{q}_{\mathbf{d}} - \mathbf{q}) \tag{3}$$

where $\ddot{\mathbf{q}}_{\mathbf{ref}}$ is the reference acceleration, $\ddot{\mathbf{q}}_{\mathbf{d}}$ is the desired acceleration obtained from trajectory $\mathbf{q}_{\mathbf{d}}$, and $\mathbf{K}_{\mathbf{p}}$ and $\mathbf{K}_{\mathbf{d}}$

IEEE Robotics and Automation Letters (RA-L) paper, presented at ICRA 2024, Yokohama, Japan. Cite as RA-L paper.

are proportional (P) and derivative (D) diagonal controller matrices with scalar gains $k_{p,i}$ and $k_{d,i}$ on the diagonals. This controller gives the linearized closed loop dynamics:

$$\mathbf{M}(\mathbf{q})\ddot{\mathbf{q}} = \mathbf{M}(\mathbf{q})\ddot{\mathbf{q}}_{\mathbf{ref}} \tag{4}$$

and the error dynamics can then be written as:

$$\ddot{\mathbf{e}} + \mathbf{K_d}\dot{\mathbf{e}} + \mathbf{K_p}\mathbf{e} = \mathbf{0} \tag{5}$$

where $\mathbf{e} = \mathbf{q_d} - \mathbf{q}$, which implies that $\mathbf{e} \to 0$ as $t \to \infty$. Error dynamics is linear with poles determined by PD gains.

B. Acceleration Control with Disturbance Observers

While computed torque control can be used for feedback linearization, it requires exact dynamic models. These models can be obtained by dynamic identification, however stability/passivity of the system may not be guaranteed [39]. For this purpose, disturbance observers can be used [40]. A disturbance observer (DOBS) [41] comprises a nominal motor model and estimates the disturbances by comparing actual and model position/velocity measurements. The estimated disturbance force is then fed back into the system, enabling the implementation of robust acceleration control. Fig. 2 shows a block diagram of disturbance observers utilized in the control of robot actuators using velocity measurements. Here, the robot is modelled in actuator space as:

$$\mathbf{M_n}\ddot{\mathbf{q}} + \underbrace{\boldsymbol{\tau_{frc}} + \boldsymbol{\tau_{int}} + \boldsymbol{\tau_{ext}}}_{\boldsymbol{\tau_{dis}}} = \boldsymbol{\tau} \tag{6}$$

where $\mathbf{M_n}$ is a diagonal mass matrix with elements $M_{n,i}$ corresponding to the nominal inertia/mass of each actuator i, $\boldsymbol{\tau_{dis}}$ is the lumped disturbance acting on the actuators, $\boldsymbol{\tau_{int}}$ is the sum of internal robot forces/torques: $\boldsymbol{\tau_{int}} = \mathbf{M}(\mathbf{q})\ddot{\mathbf{q}} - \mathbf{M_n}\ddot{\mathbf{q}} + \mathbf{C}(\mathbf{q}, \dot{\mathbf{q}}) + \mathbf{G}(\mathbf{q})$, $\boldsymbol{\tau_{frc}}$ is the friction force/torque and $\boldsymbol{\tau_{ext}}$ is the sum of all the external forces/torques acting on the actuators. The estimated disturbance on each actuator can be obtained with a disturbance observer as:

$$\hat{\tau}_{dis,i} = \frac{g_{dis,i}}{s + g_{dis,i}}(\tau_i + g_{dis,i}M_{n,i}\dot{q}_i) - g_{dis,i}M_{n,i}\dot{q}_i \tag{7}$$

where $g_{dis,i}$ is the cut-off frequency of a low pass filter used for filtering noisy velocity measurements from actuator i. It can be shown that an acceleration control system with a disturbance observer and $\tau_{ref,i} = M_{n,i}\ddot{q}_{ref,i}$ and $\tau_i = \tau_{ref,i} + \hat{\tau}_{dis,i}$, will result in the following dynamics [41]:

$$M_{n,i}s^2 q = M_{n,i}s^2 q_{ref} - G_i(s)\tau_{dis,i} \tag{8}$$

where $G_i(s) = s/(s + g_{dis,i})$ is the high-pass disturbance sensitivity function. If $\ddot{q}_{ref,i}$ is selected according to (3), closed loop error dynamics can be written for all i as:

$$(s^2 + k_{d,i}s + k_{p,i})e_i = \frac{G_i(s)\tau_{dis,i}}{M_{n,i}} \tag{9}$$

Disturbance observer compensation forces the actuator dynamics to the nominal mass dynamics within the observer bandwidth.

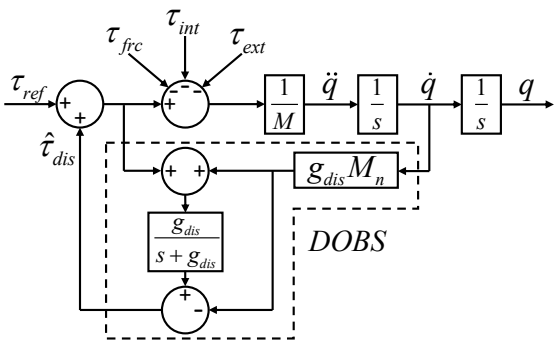

Fig. 2. Disturbance observer implementation on a single actuator with velocity measurement

C. External Force Estimation using Learning Based Dynamic Identification

It is possible to estimate external forces using disturbance observers or by torque estimates based on actuator currents [28], [29]. The dVRK Master Tool Manipulator (MTM) and Patient Side Manipulator (PSM) both have elastic transmissions and spring loading which can be hard to model parametrically and can be lumped into τ_{int} in (6).

To identify the dynamics we use deep learning. We use two neural networks for each robot, with each network responsible for identifying three degrees of freedom in actuator space. Each network has an input layer with 6 inputs that are the actuator positions and velocities. To extract important information from time-series data, we use an LSTM layer. The output of the LSTM layer, which consists of 256 hidden units, is then fed into 3 fully connected (FC) layers with ReLU activation functions. The FC layers have 256, 128 and 64 hidden neurons. The output regression layer also has 3 target outputs.

In free motion ($\boldsymbol{\tau_{ext}} = 0$), inverse dynamic torques $\boldsymbol{\tau}$ in (6), can be learned by the two networks $\mathbf{NN_m}(\mathbf{q}, \dot{\mathbf{q}})$ trained with torque measurements $\boldsymbol{\tau_m}$, or by the two networks $\mathbf{NN_{dis}}(\mathbf{q}, \dot{\mathbf{q}})$ trained with $\hat{\boldsymbol{\tau}}_{\boldsymbol{dis}}$. In the first case, the network output $\hat{\boldsymbol{\tau}}_{\boldsymbol{dyn}}$ would be $\hat{\boldsymbol{\tau}}_{\boldsymbol{dyn}} = \mathbf{NN_m}(\mathbf{q}, \dot{\mathbf{q}}) \approx \boldsymbol{\tau_m}$, and in the second case, it would be $\hat{\boldsymbol{\tau}}_{\boldsymbol{dyn}} = \mathbf{NN_{dis}}(\mathbf{q}, \dot{\mathbf{q}}) \approx \hat{\boldsymbol{\tau}}_{\boldsymbol{dis}}$.

During contact, the identified torque/disturbance $\hat{\boldsymbol{\tau}}_{\boldsymbol{dyn}}$ can be subtracted from measured torque τ_m [28], [29] (10) or the disturbance estimate $\hat{\boldsymbol{\tau}}_{\boldsymbol{dis}}$ [26] (11) to obtain the external torque estimate:

$$\hat{\boldsymbol{\tau}}_{\boldsymbol{ext}} = \boldsymbol{\tau_m} - \hat{\boldsymbol{\tau}}_{\boldsymbol{dyn}} \tag{10}$$

$$\hat{\boldsymbol{\tau}}_{\boldsymbol{ext}} = \hat{\boldsymbol{\tau}}_{\boldsymbol{dis}} - \hat{\boldsymbol{\tau}}_{\boldsymbol{dyn}} \tag{11}$$

The external forces in Cartesian space can then be obtained by applying the pseudo-inverse Jacobian transpose $\mathbf{J^{-T}}$:

$$\hat{\mathbf{F}}_{\mathbf{ext}} = \mathbf{J}^{-\mathbf{T}}\hat{\boldsymbol{\tau}}_{\boldsymbol{ext}} \tag{12}$$

D. Transparency Optimized Four Channel Control

In bilateral teleoperation, ideal performance of a control system is called transparency, and a control system should be transparent to provide perfect kinesthetic coupling between

IEEE Robotics and Automation Letters (RA-L) paper, presented at ICRA 2024, Yokohama, Japan. Cite as RA-L paper.

the operator and the environment. The two port model of a 1 DOF linearized teleoperation system can be written as:

$$Z_m v_m(s) = F_h(s) + F_{cm}(s) \tag{13}$$
$$Z_r v_r(s) = -F_e(s) + F_{cr}(s) \tag{14}$$

where Z_m, Z_r are the linearized manipulandum and remote robot impedances/dynamics, v_m, v_r are the velocities, F_h, F_e are the human and environment forces, and F_{cm}, F_{cr} are the controller efforts for the manipulandum and remote robot.

The hybrid matrix $\mathcal{H}$ can then be used to quantify the transparency of the linear teleoperation system [42]:

$$\begin{bmatrix} F_h \\ -v_r \end{bmatrix} = \underbrace{\begin{bmatrix} h_{11} & h_{12} \\ h_{21} & h_{22} \end{bmatrix}}_{\mathcal{H}} \begin{bmatrix} v_m \\ F_e \end{bmatrix} \tag{15}$$

The ideal transparency conditions are: $h_{11} = 0$, $h_{12} = 1$, $h_{21} = -1$, and $h_{22} = 0$. which imply velocity/position tracking ($v_m = v_r$) and force reflection ($F_h = F_e$) for all frequencies. The impedance transmitted to the operator by the control system, Z_{to}, can also be written as:

$$Z_{to} = \frac{h_{11} + (h_{11}h_{22} - h_{12}h_{21})Z_e}{1 + h_{22}Z_e} \tag{16}$$

where $Z_e = F_e/v_r$ is the environment impedance and, in a fully transparent system without scaling, $Z_{to} = Z_e$.

It was shown in [35] that exchange of both force and position measurements between the robots and perfect compensation of robot dynamics would be required for transparency. Such a "transparency optimized" four channel controller can be written using four communication channel parameters $C_1(s), C_2(s), C_3(s), C_4(s)$, the local force feedback channel $C_5(s), C_6(s)$, and local position controllers $C_m(s), C_r(s)$ as:

$$F_{cm}(s) = -C_4 v_r - C_m v_m - C_2 F_e + C_6 F_h \tag{17}$$
$$F_{cr}(s) = C_1 v_m - C_r v_r - C_5 F_e + C_3 F_h \tag{18}$$

It is possible to use disturbance observers with acceleration control to implement the four channel architecture [43] with $C_1 = C_r = C_p^r/s, C_4 = -C_m = -C_p^m/s$ and $C_2 = C_f^m; C_3 = C_f^r$, where $C_p^{m,r}(s) = k_p^{m,r} + k_d^{m,r}s$ are PD position controllers and $C_f^{m,r}$ are force control gains. The disturbance observer compensates the disturbances acting on the robots, including F_h, F_e, within the observer bandwidth, which can be approximated with $C_5 = C_6 = -1$. For transparency, estimated human/environment forces can be fed back with $C_5 = -1 + C_f^m; C_6 = -1 + C_f^r$. If we select $C_p^m = C_p^r = C_p$ and $C_f^m = C_f^r = C_f$ for identical robots, acceleration controllers can be written as:

$$M_n \ddot{x}_m^{ref} = C_p(x_r - x_m) + C_f(F_h - F_e) \tag{19}$$
$$M_n \ddot{x}_r^{ref} = C_p(x_m - x_r) + C_f(F_h - F_e) \tag{20}$$

where $x_m^d = x_r$, $x_r^d = x_m$, $\ddot{x}_m^d = \ddot{x}_r^d = \frac{C_f}{M_n}(F_h - F_e)$. Here, x_m and x_r are positions of manipulandum and remote robot, respectively. The hybrid parameters become: $h_{11} = \frac{M_n s}{C_f}$, $h_{12} = 1$, $h_{21} = -1$, $h_{22} = 0$. Here, h_{11} corresponds to operationality, which is the inertia of the robot felt by the operator in addition to the environment and can be decreased by increasing C_f.

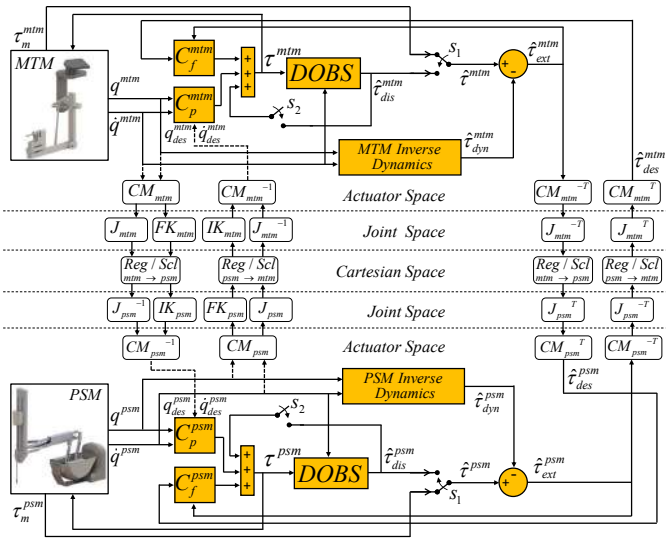

Fig. 3. Control Architecture. q: position, $\dot{q}$: velocity, τ: force/torque in actuator space, CM: coupling matrix, Reg: registration, Scl: scaling, J: Jacobian matrix, FK: forward kinematics, IK: inverse kinematics, s_1: switch to indicate current or disturbance observer based torque estimate is used, s_2: switch to indicate disturbance compensation (Cmp) is used.

E. Sensorless Four Channel Control on the dVRK

Robotic surgery requires motion scaling and a bilateral teleoperation framework has to take scaling into consideration. The master tool manipulator and patient side robots have different kinematics, dynamics and actuator torque limits so the controller goals should be first determined in Cartesian space. These goals can be written as $\mathbf{X^{mtm}} = \alpha \mathbf{X^{psm}}$ and $\hat{\mathbf{F}}_{\mathbf{ext}}^{\mathbf{mtm}} = -\beta \hat{\mathbf{F}}_{\mathbf{ext}}^{\mathbf{psm}}$, where $\mathbf{X}$ represents the Cartesian position vector, $\hat{\mathbf{F}}_{\mathbf{ext}}^{\mathbf{mtm}} \approx -\mathbf{F_h}$, $\hat{\mathbf{F}}_{\mathbf{ext}}^{\mathbf{psm}} \approx \mathbf{F_e}$ are the Cartesian external force estimates, and α, β are the scaling factors between MTM and PSM positions and forces. For these goals we propose the controller in actuator space:

$$\mathbf{M_n}\ddot{\mathbf{q}}_{\mathbf{ref}}^{\mathbf{mtm}} = \mathbf{C_p^{mtm}}(\mathbf{q_{des}^{mtm}} - \mathbf{q^{mtm}}) - \mathbf{C_f^{mtm}}(\hat{\boldsymbol{\tau}}_{\mathbf{ext}}^{\mathbf{mtm}} + \hat{\boldsymbol{\tau}}_{\mathbf{des}}^{\mathbf{mtm}})$$

$$\mathbf{M_n}\ddot{\mathbf{q}}_{\mathbf{ref}}^{\mathbf{psm}} = \mathbf{C_p^{psm}}(\mathbf{q_{des}^{psm}} - \mathbf{q^{psm}}) - \frac{\beta}{\alpha}\mathbf{C_f^{psm}}(\hat{\boldsymbol{\tau}}_{\boldsymbol{des}}^{\boldsymbol{psm}} + \hat{\boldsymbol{\tau}}_{\boldsymbol{ext}}^{\boldsymbol{psm}}) \tag{21}$$

Here we define $\mathbf{q_{des}^{mtm}} = \mathbf{CM_{mtm}}(\mathbf{IK_{mtm}}(\alpha \mathbf{X^{psm}}))$, $\mathbf{q_{des}^{psm}} = \mathbf{CM_{psm}}(\mathbf{IK_{psm}}(\frac{\mathbf{X^{mtm}}}{\alpha}))$ where $\mathbf{IK_{mtm}}, \mathbf{IK_{psm}}$ are the inverse kinematics functions, and $\mathbf{CM_{mtm}}, \mathbf{CM_{psm}}$ are the actuator coupling matrices of the MTM and PSM. $\mathbf{IK}, \mathbf{CM}$ are used for transformations from Cartesian space to actuator space. $\hat{\boldsymbol{\tau}}_{\boldsymbol{des}}^{\boldsymbol{mtm}} = \mathbf{CM_{mtm}^T}(\mathbf{J_{mtm}^T}(\beta \hat{\mathbf{F}}_{\mathbf{ext}}^{\mathbf{psm}}))$ and $\hat{\boldsymbol{\tau}}_{\boldsymbol{des}}^{\boldsymbol{psm}} = \mathbf{CM_{psm}^T}(\mathbf{J_{psm}^T}(\frac{\hat{\mathbf{F}}_{\mathbf{ext}}^{\mathbf{mtm}}}{\beta}))$ are the desired torques calculated from the external forces of the other robot and $\mathbf{J_{mtm}}, \mathbf{J_{psm}}$ are the robot Jacobians. $\mathbf{C_p}, \mathbf{C_f}$ are diagonal matrices with $C_{p,i}, C_{f,i}$ on the diagonals where $C_{p,i} = k_{p,i} + k_{d,i}s$. Either the current based torque measurement provided by the dVRK platform (10) or the disturbance observer based force estimation (11) can be used for estimation of $\hat{\mathbf{F}}_{\mathbf{ext}}^{\mathbf{mtm}}, \hat{\mathbf{F}}_{\mathbf{ext}}^{\mathbf{psm}}$ using (12). With the disturbance observer, the controller torque for each joint of the robots can then be computed as $\boldsymbol{\tau}^{\boldsymbol{mtm}} = \mathbf{M_n}\ddot{\mathbf{q}}_{\mathbf{ref}}^{\mathbf{mtm}} + \hat{\boldsymbol{\tau}}_{\boldsymbol{dis}}^{\boldsymbol{mtm}}$

IEEE Robotics and Automation Letters (RA-L) paper, presented at ICRA 2024, Yokohama, Japan. Cite as RA-L paper.

and $\boldsymbol{\tau}^{psm} = \mathbf{M_n}\ddot{\mathbf{q}}_{\mathbf{ref}}^{\mathbf{psm}} + \hat{\boldsymbol{\tau}}_{dis}^{psm}$. Fig. 3 provides a block diagram of the proposed teleoperation system.

IV. Experiment Results

A. Experiment Setup

In the experiments, we used first generation dVRK MTM and PSM units, as shown in Fig. 5. The control system software was developed with C++ using the open source cisst libraries: github.com/jhu-cisst/. The developed controller is now a part of the dVRK software stack and is shared with the dVRK community. The digital controller without neural networks can run at 1.5 kHz, however with neural networks the computer hardware was not able to execute all the loops in time so the sampling rate was reduced to 1 kHz. As in clinically deployed systems, dVRK robots are connected to the same controller to minimize time delays and IO to IO latency was measured between 1.27-3.48 ms, which is small enough to avoid stability issues. The PSM and MTM have 7 and 8 degrees of freedom respectively, and the proposed control system was designed for 6 degrees of freedom. The MTM side gripper is passive and was used to control the PSM gripper unilaterally. The redundant fourth joint of the MTM was also locked.

B. Acceleration Control System with Disturbance Observers

This experiment demonstrates the performance improvement on the dVRK using acceleration control with disturbance observers. The controller parameters were tuned manually by observing sensitivity to measurement noise and transient and steady state response analysis. The controller parameters used in the experiments are given in Table I. Experiment results containing step responses for 6 DOFs are depicted in Fig. 4, where the reference signal is indicated by the black line. The blue line represents the result without disturbance observers and the red dashed line shows the result with disturbance observers. The disturbance forces, particularly gravitational forces, have a greater impact on the coupled 2^{nd} and 3^{rd} joints as well as the wrist joints of the PSM and MTM. As can be seen from the graphs, tracking is improved with disturbance observers in both robots and steady-state errors are completely

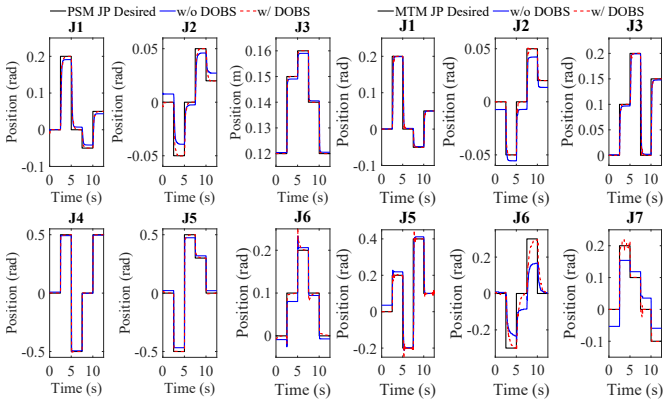

Fig. 4. Improvement in joint space position tracking with Disturbance Observers. Left: PSM, Right: MTM

TABLE I
Controller parameters used in the control system

	PSM						MTM						Units
i	**1**	**2**	**3**	**4**	**5**	**6**	**1**	**2**	**3**	**5**	**6**	**7**	-
$k_{p,i}$	20	20	800	1.5	1.5	1.5	40	40	40	0.7	0.06	0.05	-
$k_{d,i}$	4	4	56.6	0.05	0.05	0.05	5	5	5	0.05	0.03	0.0016	-
$C_{f,i}$	1	1	1	0.4	0.4	0.4	1	1	1	0.4	0.4	0.4	-
$g_{dis,i}$	10	10	10	3	3	3	10	10	10	3	3	3	rad/s
$M_{n,i}$	1e-3	1e-3	1e-3	5e-6	5e-6	5e-6	1e-3	1e-3	1e-3	5e-6	5e-6	5e-6	$kg.m^2$, kg

eliminated in most axes and significantly improved for the MTM wrist axes which have relatively weak actuators, low resolution encoders and backlash.

C. Dynamic Identification

Inverse dynamic identification for both dVRK PSM and MTM robots was performed separately. The MTM is not designed to be position controlled, therefore the implementation of an acceleration controller was crucial in the control of the MTM. Our previous identification approach [28] was also implemented on an MTM for the first time for this paper. Both networks were designed to do inference in real-time. In all experiments, the same instrument was used, which is a large needle driver, and the experiments were performed without changing the robot configuration or using a trocar, so updates were not required in the networks as in [29].

We used two separate networks for the positioning and wrist axes of each robot. For the positioning axes, the position and velocity data of first three joints, and for the wrist axes, position and velocity data of the last three joints were used. Both networks had 6 inputs and 3 outputs, and could predict the measured torques or disturbance estimates for the first three or last three axes respectively.To collect training data, each robot was bilaterally teleoperated by the other robot in free space and joint state signals for identification were collected. Data was collected for approximately 5 minutes, and 20% of this data was reserved for validation while the remaining portion was for training. The LSTM networks were trained with Tensorflow in Python, and then converted to the ONNX (Open Neural Network Exchange) format. The ONNX models were then run within the C++ code via ONNX Runtime. The normalized RMS error values for dynamic identification with measured torque and disturbance estimates were comparable and ranged from 8.5 to 13.8% for PSM and from 5.5 to 15.1% for MTM.

D. Comparison of Different Teleoperation Architectures

Extensive experiments have been conducted to evaluate the performance of different sensorless force estimation approaches and well-known teleoperation architectures. The goal of these experiments is to evaluate the transparency by comparing encoder based position tracking errors, force reflection errors between MTM/PSM force estimates, and MTM and PSM force estimates with the force sensor measurements in the Cartesian X, Y, Z axes as it is difficult to validate torque axes with the current experimental setup. To achieve impedance matching while avoiding MTM saturation, unity scaling was used: $\alpha = 1$ and $\beta = 1$. Three operators conducted two exper-

IEEE Robotics and Automation Letters (RA-L) paper, presented at ICRA 2024, Yokohama, Japan. Cite as RA-L paper.

TABLE II
NRMSE-NORMALIZED ROOT MEAN SQUARE ERRORS (STANDARD DEVIATIONS). ARCHITECTURES USED: #1: F-P, #2: P-P, #3-8: FP-FP

#	Cmp	Dyn	FE	PSM Force Estimates (%)			MTM Force Estimates (%)			Force Tracking (%)			Position Tracking (%)		
				Fx	Fy	Fz	Fx	Fy	Fz	Fx	Fy	Fz	X	Y	Z
1	-	-	τ_m	21.18(10.96)	50.62(10.06)	19.21(2.34)	17.43(6.36)	43.07(12.40)	22.05(3.97)	8.70(1.69)	7.12(0.76)	5.99(1.17)	1.65(0.44)	2.82(0.75)	2.12(0.16)
2	-	-	-	12.17(4.02)	61.35(18.36)	19.62(8.20)	19.09(3.07)	43.57(16.22)	26.59(13.52)	27.40(3.07)	22.50(9.20)	13.30(2.56)	2.56(0.63)	3.41(1.02)	2.63(0.94)
3	-	-	τ_m	26.51(13.63)	52.63(10.60)	18.52(5.85)	20.92(9.95)	45.39(10.20)	19.50(6.18)	6.84(1.35)	5.51(0.78)	4.22(0.71)	1.63(0.36)	2.83(0.95)	2.42(0.47)
4	τ_{dis}	-	τ_m	17.76(7.72)	29.55(8.95)	16.41(4.52)	17.00(1.30)	19.49(3.66)	15.65(1.75)	16.60(1.47)	14.70(2.10)	15.88(1.02)	1.04(0.13)	1.77(0.26)	1.26(0.21)
5	-	τ_m	τ_m	23.51(9.95)	23.96(7.54)	13.22(3.31)	17.18(6.75)	25.53(7.04)	18.42(3.26)	12.11(2.32)	10.33(1.66)	8.25(1.17)	1.62(0.24)	3.30(0.77)	2.57(0.56)
6	τ_{dis}	τ_m	τ_m	12.81(3.03)	20.71(7.20)	17.42(3.72)	12.96(3.01)	20.19(5.91)	14.92(2.87)	3.92(0.28)	6.37(1.15)	6.45(0.88)	0.93(0.05)	1.80(0.09)	1.07(0.10)
7	τ_{dis}	-	τ_{dis}	17.35(8.66)	27.89(4.58)	16.15(3.86)	17.94(8.86)	28.05(5.19)	16.28(3.80)	2.33(1.07)	1.37(0.37)	1.19(0.08)	0.62(0.07)	0.97(0.15)	0.53(0.09)
8	τ_{dis}	τ_{dis}	τ_{dis}	10.96(2.76)	11.25(2.14)	9.97(2.22)	12.20(2.77)	12.76(1.71)	11.06(2.92)	5.53(1.13)	6.62(0.83)	6.30(0.66)	0.81(0.06)	1.48(0.33)	1.34(0.21)

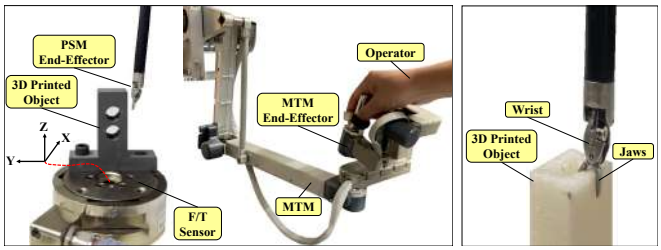

Fig. 5. Experiment setups for force estimation with the Cartesian X,Y,Z axes (Left) and wrist axes (Right)

iments with each controller. They tried to perform the same task: move the robot in free motion and contact the 3D printed force sensor apparatus on the PSM side consecutively along Z,Y,X axes (Fig. 5 (Left)). Means and standard deviations of position tracking, force reflection and force estimation/sensor errors from 6 experiments for 8 different controllers can be found in Table II. Plots comparing PSM/MTM positions and the force estimates with the F/T sensor (Gamma F/T Sensor, ATI Industrial Automation, Apex, NC, USA) measurements are presented in Fig. 6 for selected experiments. The most commonly implemented bilateral teleoperation architectures on the da Vinci systems are two channel position exchange (P-P) and position forward force feedback (F-P) controllers, and have mostly relied on force sensors or current sensing. We implemented the F-P architecture with current based force estimation (τ_m) in experiment 1 and the P-P architecture without force feedback in experiment 2 as the conventional approaches. The two architectures had similar position tracking performance and the F-P architecture had better force tracking, but was prone to instability in free motion. Then, we implemented the four channel architecture using current based force estimation (FE), without disturbance observers for compensation (Cmp) and dynamic model (Dyn) in experiment 3. With four channel teleoperation, position tracking and force reflection among the robots improved over two channel architectures, however, the comparison of the MTM/PSM estimated forces with force sensor data showed that the reflected force was not accurate. This prevents users from having a realistic sense of the environment. In experiment 4, using disturbance compensation and force estimation with measured torque together actually decreased tracking performance and in experiment 5, dynamic identification decreased force tracking performance but improved force estimation. Adding disturbance compensation in experiment 6 improved tracking and provided the best results with measured torque. Then in experiment 7, we repeated experiment 4 with disturbance observers (τ_{dis}) instead of measured torque (τ_m) for force estimation, and got the best position and force tracking results among all controllers but the force estimation errors were still relatively high. Finally, we implemented disturbance observer (τ_{dis}) based compensation (Cmp), force estimation (FE) and dynamic model (Dyn) together. This controller had the best overall performance in terms of combined force estimation and reflection. A separate experiment was conducted using this controller to show that the wrist axes can also be used to estimate forces and torques. In Fig. 5 (Right), the setup for this experiment can be seen. The operator grasped a special apparatus mounted on the force sensor and applied torques using only the wrist. Force sensor measurements along the X and Y axes and torque measurements along the Z axis were used to validate the force/torque estimation and reflection performance. Response plots and NRMSEs provided in Fig. 7 show that force/torque estimation and reflection was successfully realized along the pitch and yaw axes (corresponding to X-Y). Along the Z axis, force reflection could not be achieved as the roll actuator of the MTM has a maximum torque of 0.023 Nm, and is easily saturated. While the control system can handle impedance matching with motion scaling (e.g., $\alpha = \beta = 3$), the maximum force that can be presented to the operator is further limited by the MTM hardware.

The results show the dominating effect of surgical robot dynamics in force estimation and reflection in bilateral teleoperation. Even the transparency optimized four channel teleoperation architecture cannot provide accurate force feedback without any dynamic compensation. Our findings suggest that disturbance observer based four channel control and force estimation with deep network models can provide a comprehensive solution set for sensorless bilateral teleoperation in surgical robotics.

V. CONCLUSIONS

It was shown that the proposed sensorless four channel teleoperation framework provides higher transparency, and more accurate force feedback compared to existing two channel approaches for surgical robots. The importance of dynamic identification for external force estimation and transparency was also clearly demonstrated. A limitation for haptic feedback on the dVRK is the MTM due to low resolution encoders, weak actuation and the lack of a gripper actuator. Hardware modifications could overcome these problems. Another limitation is that the networks need to be occasionally retrained due to changes in mechanical/electrical characteristics of the

IEEE Robotics and Automation Letters (RA-L) paper, presented at ICRA 2024, Yokohama, Japan. Cite as RA-L paper.

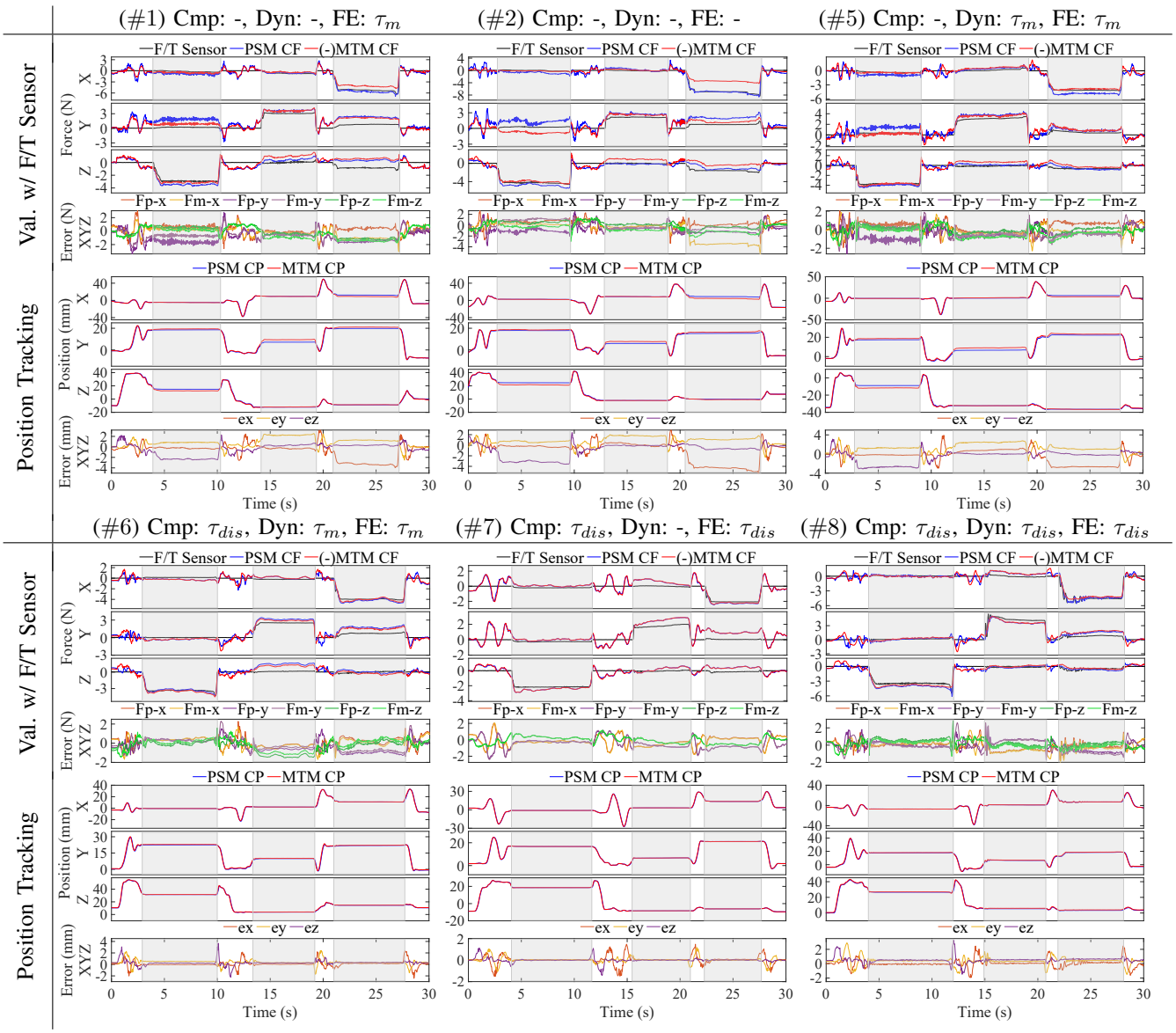

Fig. 6. Comparison of different teleoperation architectures. Shaded regions represent contact with environment. (Cmp: Compensation, Dyn: Dynamic Model, FE: Force Estimation), Architectures used: #1: F-P, #2: P-P, #5-8: FP-FP. CP: Cartesian Position, CF: Cartesian Force, {ex, ey, ez}: Position Errors in XYZ, {Fp-x, Fp-y, Fp-z},{Fm-x, Fm-y, Fm-z}: Force estimation errors in XYZ for PSM (p), MTM (m).

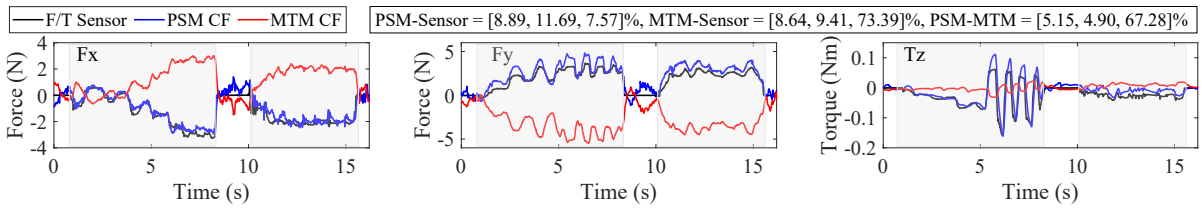

Fig. 7. Validation of external force/torque estimates for the wrist axes in Cartesian Space. Fx, Fy are forces in XY and Tz is the torque along Z.

robot over time. Transfer learning [29] can speed up this process. The proposed controller could also need manual tuning for different robots. While stability and performance of disturbance observer based control systems and four channel controllers have been studied in the literature, stability and steady state error analysis of the proposed control system with learning remains an open problem, and is a future work. One of the biggest obstacles to remote surgery is communication time delay and we would like to include time delays in our controller design using the approach in [44]. Furthermore, our method could enable dVRK users to implement other bilateral teleoperation architectures in the literature, which can easily be formulated in the four channel control framework.

REFERENCES

[1] N. Mayor, A. S. Coppola, and B. Challacombe, "Past, present and future of surgical robotics," *Trends in Urology & Men's Health*, vol. 13, no. 1, pp. 7–10, 2022.

[2] A. M. Okamura, "Haptic feedback in robot-assisted minimally invasive surgery," *Current Opinion in Urology*, vol. 19, no. 1, p. 102, 2009.

[3] R. V. Patel, S. F. Atashzar, and M. Tavakoli, "Haptic feedback and force-based teleoperation in surgical robotics," *Proceedings of the IEEE*, vol. 110, no. 7, pp. 1012–1027, 2022.

[4] H. Mayer, I. Nagy, A. Knoll, E. U. Braun, R. Bauernschmitt, and R. Lange, "Haptic feedback in a telepresence system for endoscopic heart surgery," *Presence: Teleop. and Virt. Env.*, vol. 16, no. 5, pp. 459–470, 2007.

[5] J. C. Gwilliam, Z. Pezzementi, E. Jantho, A. M. Okamura, and S. Hsiao, "Human vs. robotic tactile sensing: Detecting lumps in soft tissue," in *IEEE Haptics Symposium*, 2010, pp. 21–28.

[6] A. Abiri, S. J. Askari, A. Tao, Y.-Y. Juo, Y. Dai, J. Pensa, R. Candler, E. P. Dutson, and W. S. Grundfest, "Suture breakage warning system for robotic surgery," *IEEE Trans. BioMedical Eng.*, vol. 66, no. 4, pp. 1165–1171, 2018.

[7] A. M. Okamura, "Methods for haptic feedback in teleoperated robot-assisted surgery." *Industrial Robot*, vol. 31, no. 6, pp. 499–508, 2004.

[8] P. Kazanzides, Z. Chen, A. Deguet, G. S. Fischer, R. H. Taylor, and S. P. DiMaio, "An open-source research kit for the da Vinci surgical system," in *IEEE Int. Conf. Robot. Autom.*, 2014, pp. 6434–6439.

[9] Z. Chua and A. M. Okamura, "A modular 3-degrees-of-freedom force sensor for robot-assisted minimally invasive surgery research," *Sensors*, vol. 23, no. 11, p. 5230, 2023.

[10] P. J. Berkelman, L. L. Whitcomb, R. H. Taylor, and P. Jensen, "A miniature microsurgical instrument tip force sensor for enhanced force feedback during robot-assisted manipulation," *IEEE Trans. Robot. Autom.*, vol. 19, no. 5, pp. 917–921, 2003.

[11] U. Seibold, B. Kubler, and G. Hirzinger, "Prototype of instrument for minimally invasive surgery with 6-axis force sensing capability," in *IEEE Int. Conf. Robot. Autom.*, 2005, pp. 496–501.

[12] R. Pena, M. J. Smith, N. P. Ontiveros, F. L. Hammond, and R. J. Wood, "Printing strain gauges on Intuitive Surgical da Vinci robot end effectors," in *IEEE/RSJ Int. Conf. Intell. Robots Syst.*, Oct 2018, pp. 806–812.

[13] U. Kim, D.-H. Lee, W. J. Yoon, B. Hannaford, and H. R. Choi, "Force sensor integrated surgical forceps for minimally invasive robotic surgery," *Trans. Robot.*, vol. 31, no. 5, pp. 1214–1224, Oct 2015.

[14] J. Peirs, J. Clijnen, D. Reynaerts, H. Van Brussel, P. Herijgers, B. Corteville, and S. Boone, "A micro optical force sensor for force feedback during minimally invasive robotic surgery," *Sensors and Actuators A: Physical*, vol. 115, no. 2-3, pp. 447–455, 2004.

[15] E. Del Sol, P. Pagala, R. King, and M. Ferre, "External force estimation for telerobotics without force sensor," in *ROBOT2013:First Iberian Robotics Conf.: Adv. in Robotics, vol. 2*. Springer, 2014, pp. 631–644.

[16] A. Madhani, G. Niemeyer, and J. Salisbury, "The black falcon: a teleoperated surgical instrument for minimally invasive surgery," in *IEEE/RSJ Int. Conf. Intell. Robots Syst.*, vol. 2, 1998, pp. 936–944.

[17] M. Mahvash, J. Gwilliam, R. Agarwal, B. Vagvolgyi, L.-M. Su, D. D. Yuh, and A. M. Okamura, "Force-feedback surgical teleoperator: Controller design and palpation experiments," in *IEEE Symp. on Hapt. Interf. for Virt. Env. and Teleop. Sys.*, 2008, pp. 465–471.

[18] M. C. Lee, C. Y. Kim, B. Yao, W. J. Peine, and Y. E. Song, "Reaction force estimation of surgical robot instrument using perturbation observer with SMCSPO algorithm," in *IEEE/ASME Int. Conf. on Adv. Intell. Mechat.*, 2010, pp. 181–186.

[19] H. Sang, J. Yun, R. Monfaredi, E. Wilson, H. Fooladi, and K. Cleary, "External force estimation and implementation in robotically assisted minimally invasive surgery," *Int. J. Medical Robot*, vol. 13, no. 2, p. e1824, 2017.

[20] F. Piqué, M. N. Boushaki, M. Brancadoro, E. De Momi, and A. Menciassi, "Dynamic modeling of the da Vinci research kit arm for the estimation of interaction wrench," in *IEEE Int. Symp. on Medical Robotics (ISMR)*, 2019, pp. 1–7.

[21] J. J. O'Neill, T. K. Stephens, and T. M. Kowalewski, "Evaluation of torque measurement surrogates as applied to grip torque and jaw angle estimation of robotic surgical tools," *Robot. Autom. Lett.*, vol. 3, no. 4, p. 3027, 2018.

[22] N. Tran, J. Y. Wu, A. Deguet, and P. Kazanzides, "A deep learning approach to intrinsic force sensing on the da Vinci surgical robot," in *IEEE Int. Conf. on Robotic Computing*, 2020.

[23] G. A. Fontanelli, F. Ficuciello, L. Villani, and B. Siciliano, "Modelling and identification of the da Vinci research kit robotic arms," in *IEEE/RSJ Int. Conf. Intell. Robots Syst. (IROS)*, 2017, pp. 1464–1469.

[24] M. Haghighipanah, M. Miyasaka, and B. Hannaford, "Utilizing elasticity of cable-driven surgical robot to estimate cable tension and external force," *IEEE Robotics and Automation Letters*, vol. 2, no. 3, pp. 1593–1600, 2017.

[25] Y. Li and B. Hannaford, "Gaussian process regression for sensorless grip force estimation of cable-driven elongated surgical instruments," *IEEE Robotics and Automation Letters*, vol. 2, no. 3, pp. 1312–1319, 2017.

[26] N. Yilmaz, M. Bazman, A. Alassi, B. Gur, and U. Tumerdem, "6-axis hybrid sensing and estimation of tip forces/torques on a hyper-redundant robotic surgical instrument," in *IEEE/RSJ Int. Conf. Intell. Robots Syst. (IROS)*, 2019, pp. 2990–2997.

[27] Z. Chua, A. M. Jarc, and A. M. Okamura, "Toward force estimation in robot-assisted surgery using deep learning with vision and robot state," in *IEEE Int. Conf. Robot. Autom. (ICRA)*, 2021, pp. 12 335–12 341.

[28] N. Yilmaz, J. Y. Wu, P. Kazanzides, and U. Tumerdem, "Neural network based inverse dynamics identification and external force estimation on the da Vinci Research Kit," in *IEEE Int. Conf. Robot. Autom. (ICRA)*, 2020, pp. 1387–1393.

[29] N. Yilmaz, J. Zhang, P. Kazanzides, and U. Tumerdem, "Transfer of learned dynamics between different surgical robots and operative configurations," *Int. J. Comput. Assist. Radiol. Surg.*, vol. 17, no. 5, pp. 903–910, 2022.

[30] J. Zhang, N. Yilmaz, U. Tumerdem, and P. Kazanzides, "Learning based estimation of 7 DOF instrument and grasping forces on the da Vinci Research Kit," in *IEEE Int. Symp. on Medical Robotics (ISMR)*, 2022, pp. 1–7.

[31] M. Mahvash and A. M. Okamura, "Enhancing transparency of a position-exchange teleoperator," in *Second Joint EuroHaptics Conf. and Symp. on Hapt. Interf. for Virt. Env. and Teleop. Sys. (WHC'07)*. IEEE, 2007, pp. 470–475.

[32] M. Minelli, N. Piccinelli, F. Falezza, F. Ferraguti, R. Muradore, and C. Secchi, "Two-layer-based multiarms bilateral teleoperation architecture," *IEEE Trans. Control Syst. Technol.*, 2022.

[33] A. Tobergte, R. Konietschke, and G. Hirzinger, "Planning and control of a teleoperation system for research in minimally invasive robotic surgery," in *IEEE Int. Conf. Robot. Autom.*, 2009, pp. 4225–4232.

[34] A. Saracino, A. Deguet, F. Staderini, M. N. Boushaki, F. Cianchi, A. Menciassi, and E. Sinibaldi, "Haptic feedback in the da Vinci Research Kit (dVRK): A user study based on grasping, palpation, and incision tasks," *Int. J. Medical Robot*, vol. 15, no. 4, p. e1999, 2019.

[35] D. A. Lawrence, "Stability and transparency in bilateral teleoperation," *IEEE Trans. Robot. Autom.*, vol. 9, no. 5, pp. 624–637, 1993.

[36] M. Tavakoli, A. Aziminejad, R. V. Patel, and M. Moallem, "High-fidelity bilateral teleoperation systems and the effect of multimodal haptics," *IEEE Trans. on Sys., Man, and Cybernetics, Part B (Cybernetics)*, vol. 37, no. 6, pp. 1512–1528, 2007.

[37] D. G. Black, A. H. H. Hosseinabadi, and S. E. Salcudean, "6-DOF force sensing for the master tool manipulator of the da Vinci surgical system," *IEEE Robotics and Automation Letters*, vol. 5, no. 2, pp. 2264–2271, 2020.

[38] J. Luh, M. Walker, and R. Paul, "Resolved-acceleration control of mechanical manipulators," *IEEE Trans. Automat. Contr.*, vol. 25, no. 3, pp. 468–474, 1980.

[39] R. J. Anderson, "Passive computed torque algorithms for robots," in *IEEE Conf. on Decision and Control*, 1989, pp. 1638–1644.

[40] R. Bickel and M. Tomizuka, "Passivity based versus disturbance observer based robot control: equivalence and stability," *IFAC Proceedings Volumes*, vol. 29, no. 1, pp. 223–228, 1996.

[41] S. Komada, M. Ishida, K. Ohnishi, and T. Hori, "Disturbance observer-based motion control of direct drive motors," *IEEE Trans. Energy Convers.*, vol. 6, no. 3, pp. 553–559, 1991.

[42] B. Hannaford, "A design framework for teleoperators with kinesthetic feedback," *IEEE Trans. Rob. Auto.*, vol. 5, no. 4, pp. 426–434, 1989.

[43] W. Iida and K. Ohnishi, "Reproducibility and operationality in bilateral teleoperation," in *IEEE Int. Workshop on Adv. Mot. Ctrl (AMC)*, 2004, pp. 217–222.

[44] U. Tumerdem and K. Ohnishi, "Delay-independent L2 stability of four-channel bilateral teleoperators with damping injection," *IEEJ Trans. on Ind. Appl.*, vol. 130, no. 8, pp. 953–964, 2010.

IEEE Robotics and Automation Letters (RA-L) paper, presented at ICRA 2024, Yokohama, Japan. Cite as RA-L paper.